

SL6

CALCULATION OF INSTRUMENTAL FUNCTION

J. Drahokoupil^{1,2}

¹FJFI ČVUT, Trojanova 13, 120 00 Praha 2, ČR

²Fyzikální ústav AV ČR, v.v.i., Na Slovance 2, 182 21 Praha 8, ČR

jandrahokoupil@seznam.cz

Introduction

Current progress in computing ability enable to leave off a classical profile fitting by analytical function and compare the measured diffraction pattern with the computed one. Two main contribution exist, the former is the conduction of real structure (e.g. size, strain, ...) and the later is the proper effect of instrument to diffraction pattern. The effect related to sample in present time connected with P. Scardi and M. Leoni and their so-called whole powder pattern modeling [1]. The later one, on which is this paper focused, is mainly connected with works of A.A. Coelho and R.W. Cheary [2-5] and their fundamental parameter approach.

The instrumental function could be determined two ways. The former is by measurement of standard – sample with relatively large grains, no strains, and preferably from the same material as measured sample to avoid differences in absorption. The later possibility, which will be discussed thereafter, is to compute it.

Adequacy of convolution

The observed line profile is usually considered as a results of convolutions several appropriate function describing the particular effect to diffraction profile [2, 5-7]. For two function it is written in equation (1)

$$h(x) = g(x - y)f(y)dy \quad (1)$$

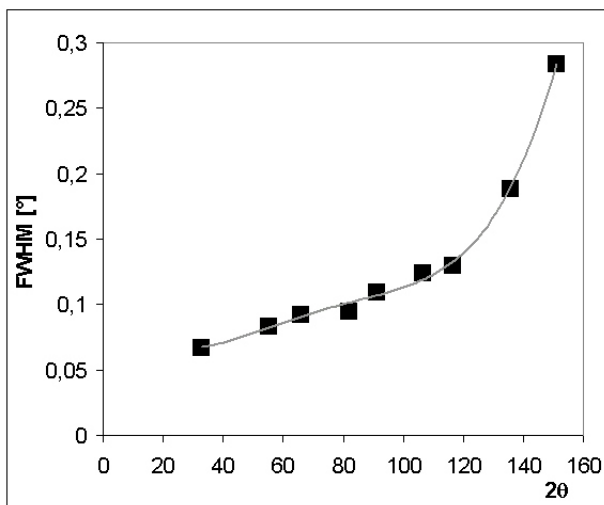


Figure 1. The FWHM vs. 2θ for CaF_2 standard measured on Brag-Brentano geometry, divergent beam, soller slits, no monochromators, Co radiation, X' Celerator – detector.

In description of X-ray diffraction line profiles are used the proper limits of integrations. When the convolution is derived, one important presumption have to be done, function g (or f , convolutions is commutative) do not change during the interval of f . Simply told, the function g is the same on the beginning and on the end of diffraction profile. If it is not true and it is not exactly true, see Fig. 1, the equation (1) should be rewritten [8]:

$$h(x) = \int_a^b g(x, y)f(y)dy. \quad (2)$$

The measured dependence of instrumental function on diffraction angle is shown on Fig. 1. It is evident that the largest effect of change is in are of high angle. Where also the K doublet is good distinguished and limits of integration have to be larger. Notwithstanding the equation (2) is not used and the computers program used convolution. This is also one of reasons why the K lines are not considered in spectral distribution, which should be taken suitable narrow.

The wavelength distribution

The knowledge of the exact shape of the source emission profile is very important in description of line profiles. In the absence of instrumental, sample and microstructural effects it represent the highest possible resolution. Earlier it was described as two Lorentzian curves having different half-widths [9,10], but it is not relevant from the physical point of view and not compatible with the observed spectral distributions. More detailed phenomenological representation of the Cu K emission profile was first published by Berger [11]. For Cr, Mn, Fe, Co, Ni and Cu the phenomenological representations are used to accurately represent the emission profiles from these elements with up to seven Lorentzians being used in some cases [12].

Geometric instrument aberrations

The most important instrument, sample, and microstructure effects contributing to powder diffraction line profiles are in Tab. 1.

Divergent beam laboratory diffractometers

The diffraction in the conventional divergent beam laboratory diffractometers is symmetric and the principal geometric aberrations contributing to a profile are i. the finite width of the x-ray source, ii. flat specimen error, iii. finite width of receiving slits, iv. specimen transparency, and v.



Table 1. The division of effects contributing to powder diffraction line profiles [5].

	Equatorial	Axial
Instrument	Target width	Soller slits
	Divergence slit angle	Target length
	Receiving slit angle	Receiving slit length
Sample	Absorption Sample thickness Tilt	Sample length
Microstructure	Crystallite size Microstrain Strain Stacking faults	

axial divergence. Primary and secondary monochromators significantly change the emission profile.

Parallel beam diffractometers

In laboratory diffractometers is the parallel beam generated by parabolic graded multilayer mirror (Göbel mirror). The beam is parallel only in equatorial plane and not in axial, so the axial divergence is present in both incident and diffracted beam. The parallelity in diffracted beam is ensured by parallel plate collimator and/or analyzer crystals and/or channel cut monochromators. There are only two main active geometric aberrations – axial divergence and finite angular acceptance of the receiving optics. Göbel mirrors and others monocrystals significantly change the emission profile of source.

Conclusions

The computation of instrumental function instead of using measured one on the standards sample brings following ad-

vantages: The standard sample is never perfect, for example grain size should be enough large to do not cause broadening and withal not to big to product continual diffraction rings. This is another problem, that often is not available standard from the same material as the sample is, what brings problem with different absorption. Next problems may be with surface roughness and packing density.

1. P. Scardi and M. Leoni, *Acta Cryst.*, **A58**, (2002), 190.
2. R. W. Cheary and A. Coelho, *J. Appl. Cryst.*, **25**, (1992), 109.
3. R. W. Cheary and A. Coelho, *J. Appl. Cryst.*, **31**, (1998), 851.
4. R. W. Cheary and A. Coelho, *J. Appl. Cryst.*, **31**, (1998), 862.
5. A. Kern, A. A. Coleho, R.W. Cheary, in *Diffraction Analysis of the Microstructure of Materials*, edited by E.J. Mittemeijer & P. Scardi (Berlin: Springer), 2004, pp. 17-50.
6. A.J.C. Wilson, *Mathematical Theory of X-ray powder Diffractometry*, Philips Technical Library. 1963.
7. H.P. Klug, L.E. Alexander, *X-Ray Diffraction Procedures*, Wiley: New York. 1974, 2nd ed..
8. M. Čerňanský, in *Defect and Microstructure Analysis by diffraction*, edited by R.B. Snyder, J. Fiala, H. J. Bunge (New York: Oxford University Press), 1999, pp. 611-651.
9. J. Ladell, W. Parrish and J. Taylor, *Acta Crystallogr.*, **12**, (1959), 561.
10. J. Finster, G. Leonhardt and A. Meisel, *J. Phys. (Paris) Colloq.*, **32**, C4, (1971), 218.
11. H. Berger, *X-ray Spectrometry*, **15**, (1986), 241.
12. G. Holzer, M. Fritsch, M. Deutsch, J. Hartwig, and E. Forster, *Phys rev. A*, **56**, (1997), 4554.

The research was supported by the project No: 106/07/0805 of the Czech Science Foundation.

SL7

Notes to moments of diffraction profiles POZNÁMKY K MOMENTŮM DIFRAKČNÍCH PROFILŮ

M. Čerňanský

Fyzikální ústav AV ČR, v. v. i., Na Slovance 2, 182 21 Praha 8, Česká republika

Na předchozím kolokviu ve Valticích bylo upozorněno na některé vlastnosti kumulantů, které lze velmi výhodně využít při analýze profilů difrakčních linií [1]. Zde se konkrétně jedná o poznatek, že pro kumulanty funkcí v konvoluci $h = f * g$ platí pro všechny řady n [2, 3]

$$n_h \quad n_f \quad n_g \quad (1)$$

Tato vlastnost kumulantů umožňuje velmi jasně formulovat již známou metodu čtvrtých momentů k určení velikosti částic D a mikrodeformací z profilu jedné difrakční linie [4]. Předpokládáme, že profily f^D a f po

řadě odpovídají velikosti částic D a mikrodeformaci a že fyzikální profil f je konvolučí profilů f^D , f . Podle (1) pak lze druhý a čtvrtý kumulant fyzikálního profilu f napsat ve tvarech

$$\begin{array}{ccccc} & & D & & \\ & 2 & & 2 & \\ a & & & & 2 \\ & & D & & \\ & 4 & & 4 & \end{array} \quad (2)$$

kde ${}_2^D$ a ${}_4^D$ jsou druhý a čtvrtý kumulant profilu f^D , podobně k_2 a k_4 jsou druhý a čtvrtý kumulant profilu f .



Z obecných vztahů mezi kumulanty a centrálními momenty [5]

$$\begin{matrix} 2 & 2 \\ 4 & 4 \end{matrix} \quad 3 \quad 2 \quad (4)$$

$$(5)$$

a pak vychází

$$a \quad \begin{matrix} D & D \\ 2 & 2 \end{matrix}, \quad \begin{matrix} D & D \\ 4 & 4 \end{matrix} \quad 3\left(\frac{D}{2}\right)^2 \quad (6)$$

$$2 \quad 2, \quad 4 \quad 4 \quad 3\left(\frac{D}{2}\right)^2. \quad (7)$$

Rovnice (2) a (3) tvoří soustavu dvou rovnic pro dvě neznámé – velikost částic D a mikrodeformaci α . Tyto neznámé se v (2) a (3) explicitně objeví po dosazení centrálních momentů z pravých stran v (6) a (7). Existuje totiž vztah [6]

$$W = k \cdot (2) / (2^2 D \cos \alpha), \quad (8)$$

kde W je variance, t.j. druhý centrální moment $\frac{D}{2}$ profilu f^D , k je faktor tvaru částic a Millerových indexů, (2) je úhlový interval pro výpočet variance, α je vlnová délka a α_0 je Braggův úhel. Podobně profil f má druhý centrální moment [6]

$$2 \quad 4 \left\langle \frac{D}{2} \right\rangle \tan^2 \alpha_0. \quad (9)$$

Než se provede zmíněné dosazení, je dobré si uvědomit následující skutečnosti. Obvykle se o profilu f předpokládá, že má Gaussův tvar [7]. Navíc bylo ukázáno, že čtvrtý kumulant Gaussovy funkce je roven nule [8]. Tyto skutečnosti vedou k podstatnému zjednodušení při řešení soustavy rovnic (2) a (3) pro neznámou velikost částic D a neznámou mikrodeformaci α .

Ukazuje se, že důležité jsou zejména dva případy: a) čtvrtý centrální moment profilu f^D od velikosti částic je přímo úměrný druhému centrálnímu momentu tohoto profilu, b) čtvrtý centrální moment profilu f^D je přímo úměrný druhé mocnině druhého centrálního momentu tohoto profilu. Pomocí první věty integrálního počtu o střední hodnotě [9] se dá obecně dokázat, že nastává varianta a). Zmíněná věta zní: Jsou-li funkce $f(x)$ a $g(x)$ v intervalu $\langle a, b \rangle$ spojité a má-li funkce $g(x)$ v tomto intervalu stále totéž znaménko, platí

$$\int_a^b f(x)g(x)dx = f(\frac{a+b}{2}) \int_a^b g(x)dx \text{ pro } a < x < b, \quad (10)$$

kde x je hodnota z intervalu (a, b) . Dosadíme tedy $f(x) = x^2$ a $g(x) = x^2(x)$, kde (x) je profil difrakční linie. Předpoklady věty jsou evidentně splněny, takže podle definice druhého a čtvrtého centrálního momentu vychází

$$4 \quad K \quad 2 \quad (11)$$

Pro Gaussovou křivku sice platí

$$4 \quad L(\frac{D}{2})^2, \quad (12)$$

ale nemůžeme předpokládat, že oba profily, f^D, f současně mají Gaussův tvar, protože to by při řešení soustavy (2), (3) vedlo k neurčitým výrazům typu 0/0.

Druhá poznámka se týká tvaru závislosti momentu profilu f^D od velikosti částic D na této veličině (D). Podle známého Wilsonova vzorce (8) je variance profilu f^D nepřímo úměrná velikosti částic D . Variance je podle definice druhým centrálním momentem profilu. Profil od velikosti částic má často tvar [10]

$$f(s) = \sin^2(\pi s) / (\pi s)^2, \quad (13)$$

kde $s = 2 \sin \alpha_0 / \lambda$ je proměnná profilu v reciprokém prostoru a M je počet difrakujících rovin ve směru kolmém na tyto roviny. Velikost částic D je zřejmě M – násobkem příslušné mezirovinné vzdálenosti. Přímý výpočet variance profilu $f(s)$, daného rovnicí (13), podle definice z matematické statistiky [5], dává

$$W = \frac{1}{m_0} \int_{m_0}^b (s - m_1)^2 f(s) ds = \frac{1}{(M)} \quad (14)$$

kde m_0 je v našem případě integrální intenzita a m_1 těžiště profilu. V tomto případě tedy vychází, že variance profilu od velikosti částic je nepřímo úměrná druhé mocnině velikosti částic.

1. M. Černanský: *Materials Structure*, 15 (2008) k45-k46.
2. A.C. Aitken: *Statistical Mathematics*. Edinburgh and London 1947. Oliver and Boyd.
3. L. Janossy: *Theory and Practice of the Evaluation of Measurements*. Oxford 1965. Oxford University Press.
4. A.S. Kagan & V.M. Snovidov: *Fizika metallov i metallovedenije*, 19 (1965) 191-198.
5. H. Cramér: *Mathematical Methods of Statistics*. Princeton 1946. Princeton University Press.
6. H.P. Klug & L.E. Alexander: *X-Ray Diffraction Procedures for Polycrystalline and Amorphous Materials*. New York 1974. Wiley, 2nd ed.
7. B.E. Warren: *Prog. Met. Phys.* **8**, (1959) 147-202. Eds. B. Chalmers & R. King. London: Pergamon Press. Ruský překlad *Usp. Fiz. Met.* **5** (1963) 172-237.
8. M. Čerňanský: *Zeit. Kristallogr. Supplement* No. 27 (2008) 127-133.
9. H.-J. Bartsch: *Matematické vzorce*. Praha 1983. SNTL.
10. Guinier, A. (1963). *X-Ray Diffraction*. San Francisco and London 1963. Freeman.

Poděkování. Tato práce vznikla v rámci realizace projektu Grantové agentury České republiky, číslo 106/07/0805.



SL8

INFLUENCE OF PROTECTIVE GAS ON THE PHASE COMPOSITION OF Mg-Ni-Fe-H BASED NANOCOMPOSITE PREPARED BY SPARK SYNTHESIS

P. Roupcová^{1, 2}, O. Schneeweiss¹

¹Institute of Physics of Material, Czech Academy of Science, v.v.i., Brno, Czech Republic

²Institute of Materials Engineering, Brno University of Technology, Technická 2, 616 69 Brno, Czech Republic, roupcova@ipm.cz

The metallic composites based on Mg(MgO) with 3d metals containing nanocrystalline particles belong to the most expected candidates for hydrogen storage materials. Their practical application, however, are connected with some difficulties due to high temperature of hydrogen desorption and relatively slow kinetics of absorption and desorption. This disadvantage could be overcome if these alloys would be applied in a nanocrystalline form. The nanocrystalline alloys or composites exhibit much faster kinetics of hydrogen absorption and desorption and lower temperature of hydriding/dehydriding conventional crystalline materials with the same composition [1-3]. The metallic hydride based on Mg-TM and their nanocrystalline form is promising the improvement of properties. The MgH₂ contains approximately 7.6 wt. % hydrogen but its high stability ($H = -75\text{ kJ mol}^{-1}$) and high pressure of 0.18 MPa at 300°C limit its usage to high-temperature hydride applications [4]. Mg₂FeH₆ on the other hand has a hydrogen capacity higher than Mg₂NiH₄, 6.7 wt. % and 3.6 wt. %, respectively [5]. However, the Mg-Fe intermetallic compound exists only in the hydride form [6]. The most attempts carried out to form Mg-Fe alloys or intermetallic compound were based on mechanical alloying, but observed an increase in solubility of Fe in Mg was very low [3, 5].

Spark erosion was performed in the two types of chamber. The first shows in the Fig. 1 do not provide the handling in protective atmosphere. This synthesis is a possible alternative among the methods for preparing a new Zr-Fe phase simultaneously yielding nanocrystalline particles. This method was used for the preparation of amorphous, nanocrystalline or crystalline powder materials. The conditions of erosion are characterised by high temperature (above 10⁴ K) and pressure (~ 280 MPa) in a plasma channel, where a synthesis of the materials of electrodes with the surrounding occurs, and high cooling rate (~10⁸ K s⁻¹) [7-8]. It allows to overcome the solubility limits reached by classic alloying treatments and to synthesize new materials.

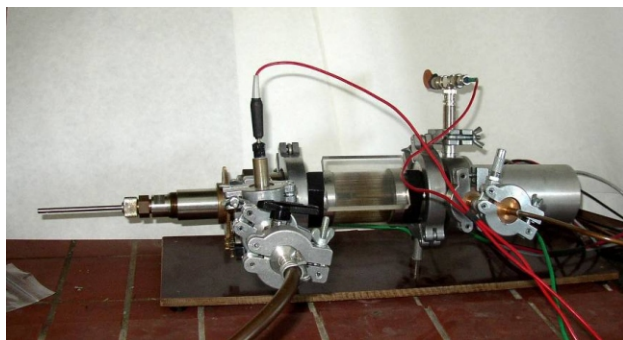


Figure 1. The spark synthesis chamber works in floating gas.

Moreover, there are some possibilities to modify its composition by varying the parameters of sparks (e.g., voltage or time) and/or chemical composition, temperature and density (pressure) of the gaseous or liquid dielectrics. The nanopowder was prepared by spark synthesis of electrodes of pure Mg (99.9 %) and Ni-Fe (99.9 %) in a hydrogen (5N) and hydrogen 10 % - argon 90 % atmosphere serving as dielectric [9-10]. The results obtained on samples handled in air were compared with the samples hold in envelopment with protective atmosphere.

The structure of the samples was checked by X-ray diffraction (XRD) using X'Pert diffractometer and CoK radiation with qualitative analysis carried out by HighScore® software and the JCPDS PDF-4 database. For a quantitative analysis HighScore plus® with Rietveld structural models based on the ICSD database was applied. ⁵⁷Fe Mössbauer spectra were collected by a standard transmission method at room temperature using a ⁵⁷Co/Rh source. The calibration of the spectra is referred relative to

-Fe at room temperature. The computer processing of the spectra was done by the CONFIT package [11] yielding by intensities I of the components (atomic fraction of Fe atoms), their hyperfine fields B_{hf} , isomer shifts and quadrupole splittings .

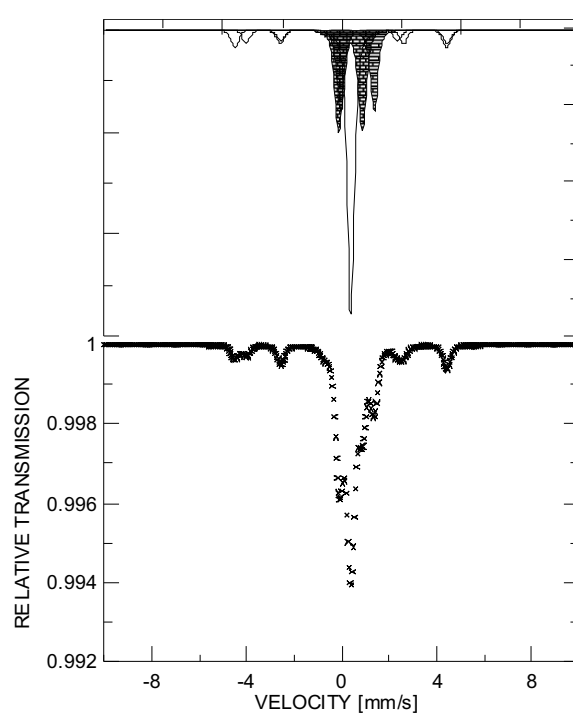


Figure 2. Powder handled in air.

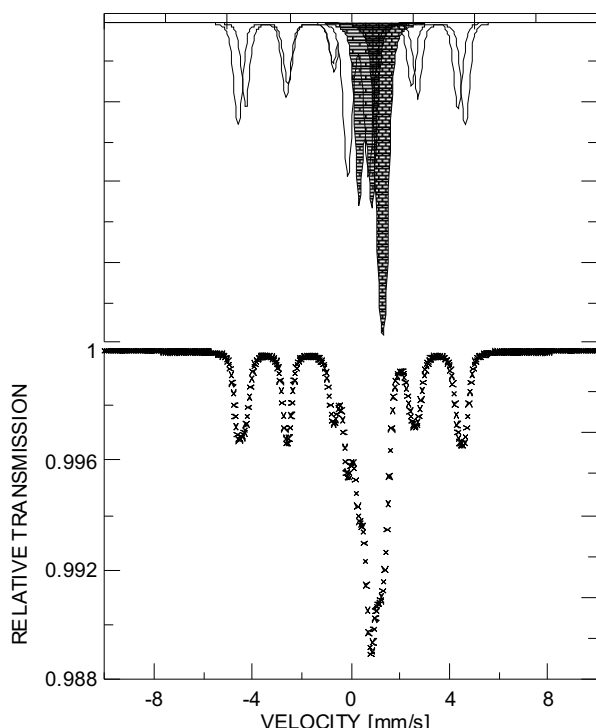


Figure 3. Powder handled in CO.

The TG/DTA results indicate presence of hydrides and high adsorption capacity of moisture and air gases. We optimize handling of powder sample in various protected atmospheres due its high sensitivity to oxidation and the trapping moisture and small molecule of gases from air. The most significant problems were: purity of gases, size of gasses molecules and absorption of X-rays. Although ability CO to protect the nanopowder against oxidation was partial only, it was determined the most effective gas. The XRD measurement observed FeNi₃ and MgO phases in the all types of as-prepared samples handled in air and in protected gasses except the argon atmosphere. The Mössbauer

spectra show in figure 2 and 3 differences of amount of iron oxide phases. The sample handling in air contains 18.7 atomic fraction (a. f.) of FeNi₃ and 81.3 a. f. of iron oxides phases. The sample protected by CO shows 43.9 a. f. of FeNi₃ and residuum of iron oxides. XRD shows 2.3 wt. % FeNi₃ and 97.7 wt. % MgO in sample handled in air and 12.5 wt. % FeNi₃ and 87.5% wt. % in CO.

1. W. Liu, H. Wu, Y. Lei et all. *J. Alloys Comp.*, **261** (1997) 289.
2. T. Spassov, U. Köster, *J. Alloys Comp.*, **287** (1999) 243.
3. L. E. A. Berlouis, E. Cambera, E. Hall-Barrientoss et all., *J. Mater. Res.*, **16** (2001) 45.
4. K. H. J. Bushow, P. C. P. Bouten, A. R. Miedema, *Rep. Prog. Phys.*, **45** (1982) 937.
5. J. Huot, H. Hayakawa, E. Akiba, *J. Alloys Comp.*, **248** (1997) 164.
6. J. J. Didissheim, P. Zolliker, K. Yvon et all. *Inorg. Chem.*, **23** (1984) 1953.
7. A. Zaluska, L. Zaluski, J. O. Strom-Olsen, *Appl. Phys. A.*, **72** (2001) 157.
8. L. Chen, F. Wu, M. Tong, B. R. Long, Z. Q. Shang, H. Liu, W. S. Sun, K. Yang, L. B. Wang, Y. Y. Li, *J. Alloys Comp.*, **293** (1999) 508.
9. J. L. Walter, *Powder Metall.*, **31** (1988) 267.
10. A. E. Berkowitz, J. L. Walter, *Mater. Sci. Eng.*, **55** (1982) 275.
11. T. Žák, in *Mössbauer Spectroscopy in Materials Science*, edited by M. Miglierini and D. Petridis (Dordrecht: Kluwer), 1999, p. 385.

This work was supported by the Czech Ministry of Education, Youth and Sports (1M6198959201), Academy of Sciences of the Czech Republic (AV0Z20410507) and Grant Agency of the Czech Republic 106/09/P556.

SL9

FEROMAGNETICKÁ SLITINA S TVAROVOU PAMĚTÍ Co₃₈Ni₃₃Al₂₉ - PŘÍPRAVA MONOKRYSTALŮ A JEJICH CHARAKTERIZACE

Jaromír Kopeček¹, Karel Jurek², Markéta Jarošová², Jan Drahokoupil¹, Silvie Sedláková-Ignácová¹, Petr Šittner¹ a Václav Novák¹

¹Fyzikální Ústav AV ČR, v.v.i., Na Slovance 2, CZ-182 21 Praha

²Fyzikální Ústav AV ČR, v.v.i., Cukrovarnická 10, CZ-162 53 Praha

Magnetickým polem řízené slitiny s tvarovou pamětí (FSMA) představují širokou aplikaci oblast. Jakkoli fázová transformace probíhající vlivem změny/přítomnosti magnetického pole, či pouhá reorientace strukturní domény (varianty), jistě není nicméně neznámým, výrazná makroskopická změna tvaru (v řádu procent) je jistě pozoruhodná. V současné době patří k nejlépe prostudovaným a aplikovaným slitinám na bázi intermetalika Ni₂MnGa.

Mezi další potenciální kandidáty použitelnosti patří také slitiny na bázi CoNiAl, které jsou zvláště pro aplikaci sféru atraktivní hlavně vyššími transformačními napětími. Vzdor tomu, že jsou kobaltové slitiny studovány dlouhá desetiletí, naráží studium FSMA na tradiční problémy, se kterými se potýkala již metalurgie od padesátých let: Intermetalická fáze B2 (Co,Ni)Al - matrice slitiny, ve které dochází k martenzitické transformaci je extrémně křehká a praská. Bylo zjištěno, že kompenzaci nežádoucích napětí



napomáhá přítomnost -fáze (fcc kobaltu s příměsí ostatních složek slitiny). Pro studium martenzitické transformace je proto třeba připravit směrově krystalizované vzorky s „monokrystalickou“ B2-maticí a s homogenní distribucí částic -fáze. Tyto vzorky jsou připravovány pomocí metod používaných pro růst monokrystalů - Bridgmanovy metody a metody zonální tavby. Z nich jsou následně připraveny vzorky pro deformační zkoušky,

SL10

USEFUL DISORDER

Jana Klimentová, Pavel Vojtíšek*, Jan Kotek

Department of Inorganic Chemistry, Faculty of Science, Charles University, Hlavova 2030, Prague 2, 128 43, Czech Republic, pavojt@natur.cuni.cz

Coordination chemistry of lanthanide ions with *N,O*-macrocyclic ligands is widely investigated because of the importance of their medicinal and biochemical use, such as Gd³⁺ complexes as contrast agents (CA) in magnetic resonance imaging (MRI) [1,2], ⁹⁰Y complexes in radioimmunotherapy [2] and the Eu³⁺ and Tb³⁺ compounds as the luminescence probes [2,3]. Previously, we published [4] an interesting set of structures of complexes of 1,4,7,10-tetraazacyclododecane-10-methyl-1,4,7-tris(methylene-phenylphosphinic) acid ($H_3\mathbf{L}^1$, see Figure 1). This acid forms neutral dimeric complexes $[Ln(\mathbf{L}^1)(H_2O)_n]_2 \cdot xH_2O \cdot yMeOH$ with Ln³⁺ ions, where $n = 0$ or 1, $x = 5-7$ and $y = 0-2$, for different Ln³⁺ [4]. All compounds are isostructural and crystallise in space group $P2_1/c$ (no. 14) with similar values of lattice parameters and similar position of the lanthanide ion in the unit cell.

However, the compound $[Pr(\mathbf{L}^1)(H_2O)_{1,33}]_2 \cdot 27.5H_2O$ does not belong to the previously published isostructural set. The structure investigation of $[Pr(\mathbf{L}^1)(H_2O)_{1,33}]_2 \cdot 27.5H_2O$ has resulted in an interesting conclusion [5]. The successful modelling of disorders in the case gave us a picture of “frozen solution” with samples of isomeric species present. Three chemically and four crystallographically different complexes were identified and structurally characterised:

$[Pr(\mathbf{L}^1-R,S)]_2$ with coordination number (CN) 8, $[Pr(\mathbf{L}^1-R,R)(H_2O)]_2$ with CN 9 and two species

v nichž je žíháním a následným zakalením nastavena teplota martenzitické transformace, která je termomechanickou historii vzorku citlivá. Struktura připravených vzorků je studována pomocí optické metalografie, SEM s detektory EDX a EBSD. Diskutovány jsou parametry přípravy vzorků a vliv žíhání.

$[Pr(\mathbf{L}^1-R,S)(H_2O)]_2$ with CN 9, but with a little different geometrical parameters (the symbols \mathbf{L}^1-R,R or \mathbf{L}^1-R,S mean the same or different chirality on ligand phosphorus atoms P1 and P2 in the complexes (P3 belongs to a bridging phosphinic group). Therefore, the title compound should be written as $0.67[Pr(\mathbf{L}^1-R,R)(H_2O)]_2 \cdot 0.33[Pr(\mathbf{L}^1-R,S)(H_2O)]_2 \cdot 0.67[Pr(\mathbf{L}^1-R,S)]_2 \cdot 0.33[Pr(\mathbf{L}^1-R,S)(H_2O)]_2 \cdot 27.5H_2O$.

Compound $[Y(H\mathbf{L}^2)(H_2O)][Y(H\mathbf{L}^2)] \cdot 6H_2O \cdot iPrOH$, where $H_4\mathbf{L}^2$ is 1,4,7,10-tetraazacyclododecane-1,4,7-triacetic-10-methyl(4-aminobenzylphosphinic) acid (Figure 1), was prepared in the solid state and studied using X-ray crystallography [6].

In contrast to all single-crystal structures of complexes of other H_4 dota-like ligands published before, the structure has been “disordered” also in the macrocyclic part. The successful modelling of disorders in this case showed three distinct units found in one cell: two species adopting a twisted-square antiprismatic configuration with ($TSA - CN 9$) and without ($TSA' - CN 8$) coordinated water molecule, $[Y(H\mathbf{L}^2)(H_2O)]$, $[Y(H\mathbf{L}^2)]$, and one isomer with a square antiprismatic configuration ($SA - CN 9$), $[Y(H\mathbf{L}^2)(H_2O)]$. In addition, this is the first complex with the H_4 dota-like ligand for which the structures of three possible species were determined in the solid state [6]. It can be interpreted again as a picture of “frozen solution” with samples of isomeric (conformeric) species present.

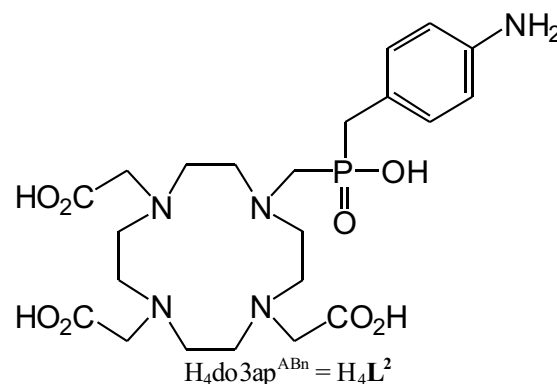
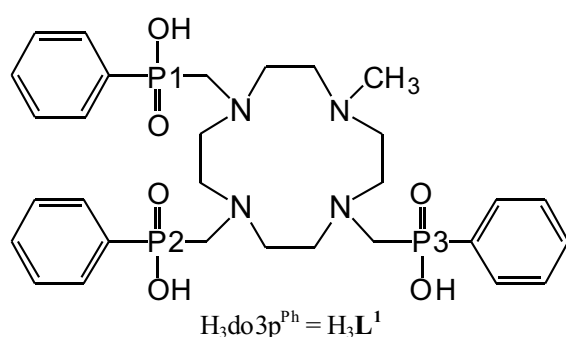


Figure 1. Structures of the ligand discussed.

In our opinion, both examples mentioned above illustrate that disorder can represent not only a nuisance in structure solving and refinement; it may bring useful chemical information as well.

1. The Chemistry of Contrast Agents in Medical Magnetic Resonance Imaging, eds. A. E. Merbach, É. Tóth, Wiley, Chichester, U. K. (2001); Topics in Current Chemistry, Springer, Frankfurt am Main, Germany **221** (2002).
2. D. Parker, in Comprehensive Supramolecular Chemistry, ed. J.-M. Lehn, Pergamon, Oxford, **10** (1996) 487.

3. S. Faulkner, J.L. Matthews, in Comprehensive Coordination Chemistry II, eds. J.A. McCleverty, T. J. Meyer, Elsevier, Amsterdam **9** (2004) 913 and refs therein.
4. J. Rohovec, P. Vojtíšek, I. Lukeš, P. Hermann, J. Ludvík, *J. Chem. Soc., Dalton Trans.* (2000) 141–148.
5. J. Klimentová, P. Vojtíšek, *J. Mol. Struct.* **826** (2007) 82–88.
6. J. Kotek, J. Rudovský, P. Hermann, I. Lukeš, *Inorg. Chem.* **46** (2006) 3097–3102.

SL11

POLYMORPHISM, ISOMORPHISM, DISTORTION AND SUPRAMOLECULAR ISOMERISM OF COMPLEXES $[\text{Cu}(\text{RCOO})_2(\text{dena})_2(\text{H}_2\text{O})_2]$ (DENA = N,N-DIETHYLNICOTINAMIDE)

J. Moncol[†], M. Koman, D. Valigura

Department of Inorganic Chemistry, Faculty of Chemical and Food Technology, Radlinského 9, SK-812 37 Bratislava, Slovakia, jan.moncol@stuba.sk

N,N-Diethylnicotinamide (dena) [1] is an important respiratory stimulant. It is metabolized rapidly to nicotinamide, one of metabolite of vitamin B₃ – niacin. The coordination of the dena ligand occurs *via* the pyridine ring nitrogen atom and other possible donor atoms for coordination bonds are less preferred. This preferential bonding can be seen on the basis of the structural data found in the CSD database [2]. Some copper(II) carboxylato complexes with *N,N*-diethylnicotinamide were also studied by X-ray. They exhibit dimeric, monomeric or polymeric structures, and the *N,N*-diethylnicotinamide is predominantly coordinated as monodentate pyridine-like N-donor ligand and only a few examples of bridging bonding mode could be found.

The most frequent copper(II) carboxylate complexes with *N,N*-diethylnicotinamide have general formula $[\text{Cu}(\text{RCOO})_2(\text{dena})_2(\text{H}_2\text{O})_2]$, where RCOO is 2-nitrobenzoate (**1**) [3]; 2-chlorobenzoate (**2**) [4]; 2-bromobenzoate (**3**) [4]; 4-nitrobenzoate (**4**) [5]; 2-chloronicotinate (**5**) [6]; 4-methoxysalicylate (**6**) [7]; 3-methylsalicylate (**7,8**) (Figure 2) [7]; 5-methoxysalicylate (**9**) [7], flufenamate (**10**) [8]; mefanamate (**11**) [9]; tolfenamate (**12**) [10] and 3-methoxysalicylate [11] in $[\text{Cu}(3-\text{MeOSal})_2(\text{dena})_2(\text{H}_2\text{O})_2] \cdot 2\text{H}_2\text{O}$ (**13**). The coordination environment of the copper atom of all ten compounds is elongated tetragonal bipyramidal, The tetragonal plane of is built up by a pair of unidentate carboxylate anions using carboxylate oxygen atoms [$\text{Cu}-\text{O}_{\text{eq}}$ in the range 1.96–1.99 Å] and by a pair of neutral *N,N*-diethylnicotinamide molecules using pyridine ring nitrogen atoms [$\text{Cu}-\text{N}_{\text{eq}}$ in the range 1.99–2.04 Å] in *trans* positions. The axial positions are occupied by the coordinated water molecules [$\text{Cu}-\text{Ow}_{\text{ax}}$ in the range 2.41–2.52 Å].

Intramolecular hydrogen-bonding interactions involving an axial coordinated water molecule and uncoordinated carboxylate oxygen atom stabilize the molecular structures on all complexes. The molecules of the complexes **1–12** are linked to adjacent molecules through intermolecular hydrogen-bonds between coordinated water molecules and

uncoordinated oxygen atoms of *N,N*-diethylnicotinamide, and they create two-dimensional supramolecular hydrogen-bond networks in iso-structural monoclinic complexes **1–3**, or one-dimensional supramolecular hydrogen-bond chains in two different groups of iso-structural triclinic complexes complexes **4–7** and **8–9**. The two groups of triclinic complexes present variability of - stacking interactions between two pyridine rings of *N,N*-diethylnicotinamide and possible orientations of supramolecular hydrogen-bond chains. The both polymorphs of complex $[\text{Cu}(3-\text{MeSal})_2(\text{dena})_2(\text{H}_2\text{O})_2]$ (**7**) and (**8**) exists in triclinic form and it is example of supramolecular isomerism [12]. The crystal structures of complex $[\text{Cu}(4-\text{MeOSal})_2(\text{dena})_2(\text{H}_2\text{O})_2]$ (**6**), measured at two temperatures, gave evidence of the distortion isomerism [13] in this complex. The crystal structures of monoclinic complexes **10–12** consist of

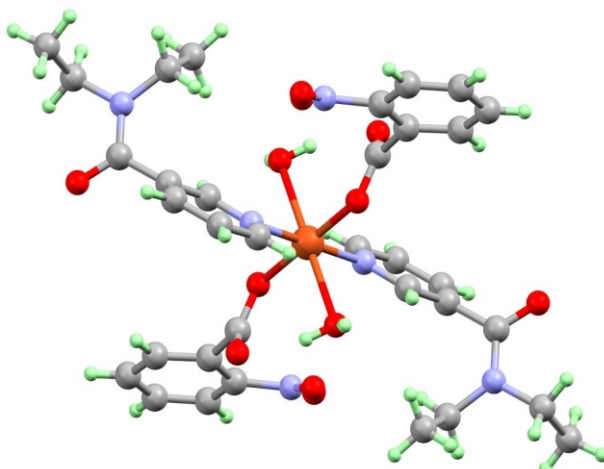
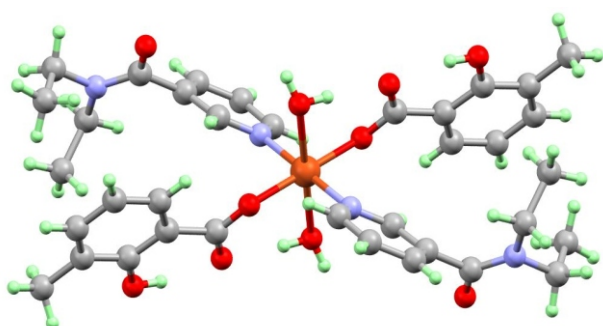
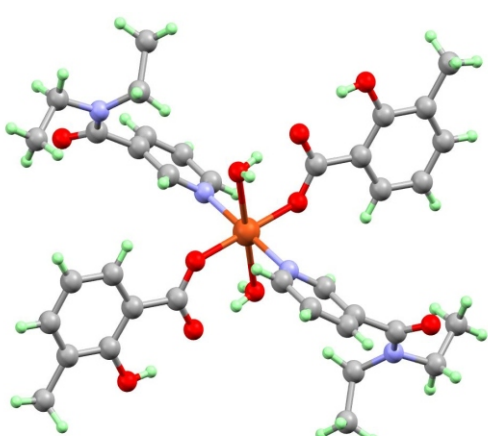


Figure 1. Molecular structure of $[\text{Cu}(2-\text{NO}_2\text{Bz})_2(\text{dena})_2(\text{H}_2\text{O})_2]$ (1).



(7)



(8)

Figure 2. Molecular structures of two polymorphs of $[\text{Cu}(3\text{-MeSal})_2(\text{dena})_2(\text{H}_2\text{O})_2]$ (7) and (8).

complex molecules linked to one-dimensional supramolecular chains by intermolecular hydrogen-bonds, but the carboxylate anions are more complicated and crystal structures are different in comparison with triclinic complexes. The crystal structure of monoclinic complex $[\text{Cu}(3\text{-MeOSal})_2(\text{dena})_2(\text{H}_2\text{O})_2] \cdot 2\text{H}_2\text{O}$ (13) consists of complex

molecules as well as uncoordinated water molecules, linked to enriched hydrogen-bond networks.

We thank Scientific Grant Agency of the Ministry of Education of Slovak Republic and the Slovak Academy of Sciences for financial support (1/4454/07).

1. L.B. Zavodnik, V.M. Tsyrkumov, M.I. Bushma, P.I. Lukienko & L.F. Legonkova, *Farmakol. Toksikol.*, **54**, (1991), 69.
2. F.A. Allen, *Acta Cryst.*, **B58**, (2002), 380.
3. J. Kavalírová, M. Korabik, P. Stachová, J. Moncol, R. Sillanpää, T. Lis, D. Mikloš, M. Melník, J. Mroziński & D. Valigura, *Polyhedron*, **27**, (2008), 1333.
4. J. Kavalírová, D. Valigura & J. Moncol, *Insights into Coordination, Bioinorganic and Applied Inorganic Chemistry*, Ed. M. Melník, P. Segl'a, M. Tatarko, Press of Slovak University of Technology, Bratislava, 2009, p. 133.
5. T. Hökelek, K. Budak, K. Sendil & H. Necefoglu, *Acta Cryst.*, **C54**, (1997), 347.
6. J. Moncol, M. Palicová, P. Segl'a, M. Koman, M. Melník, M. Valko & T. Głowiąk, *Polyhedron*, **21**, (2002), 365.
7. Z. Repická, J. Moncol, L. Krupková, D. Hudecová, M. Korabik & D. Valigura, *Insights into Coordination, Bioinorganic and Applied Inorganic Chemistry*, Ed. M. Melník, P. Segl'a & M. Tatarko, Press of Slovak University of Technology, Bratislava, 2009, p. 287.
8. M. Melník, I. Potočnak, L. Macášková, D. Mikloš & C.E. Holloway, *Polyhedron*, **15**, (1996), 2159.
9. M. Melník, M. Koman, L. Macášková & T. Głowiąk, *J. Coord. Chem.*, **44**, (1998), 163.
10. Š. Lörinc, J. Svorec, J. Moncol, M. Melník & M. Koman, *Transition Met. Chem.*, to submitted.
11. J. Moncol, Z. Pučeková, T. Lis & D. Valigura, *Acta Cryst.*, **E62**, (2006), m448.
12. B. Moulton & M.J. Zaworotko, *Chem. Rev.*, **101**, (2001), 1629.
13. J. Gažo, *Pure Appl. Chem.*, **38**, (1974), 279."

SL12

STRUCTURE OF VALINOMYCIN AND ITS COMPLEXES

Jindřich Hašek^{1*}, Emanuel Makrlík², Michal Dušek³, Ivana Císařová⁴, Jan Dohnálek¹, Jarmila Dušková¹, Tereza Skálová¹

¹Institute of Macromolecular Chemistry, AS CR, Heyrovského nám.2, 162 06 Praha 6,

²Faculty of Applied Sciences, University of West Bohemia, Husova 11, 30614 Plzeň,

³Institute of Physics, Academy of Sciences of CR, Cukrovarnická 2, 16000 Praha 6,

⁴Institute of Inorganic Chemistry, Charles University, Hlavova 2030, 128 40 Praha 2
hasek@imc.cas.cz

Introduction

Valinomycin is a cyclic dodecadepsipeptide composed of twelve -aminoacid-like residues, all with hydrophobic side chains. More accurately, it can be described as a trimer [Val – ODVal –DVal - OAla]₃, where Val is for L-valine, ODVal for deamino-oxy-D-valine, DVal for

D-valine and OAla for deamino-oxy-L-alanine. The chemical composition of valinomycin gives it a principle importance in any living organisms because of its role in selective transport of ions across the cell membranes. The Cambridge structure database of organic and organometallic compounds [1] contains 20 records, 16 of them representing independent observations. All structures

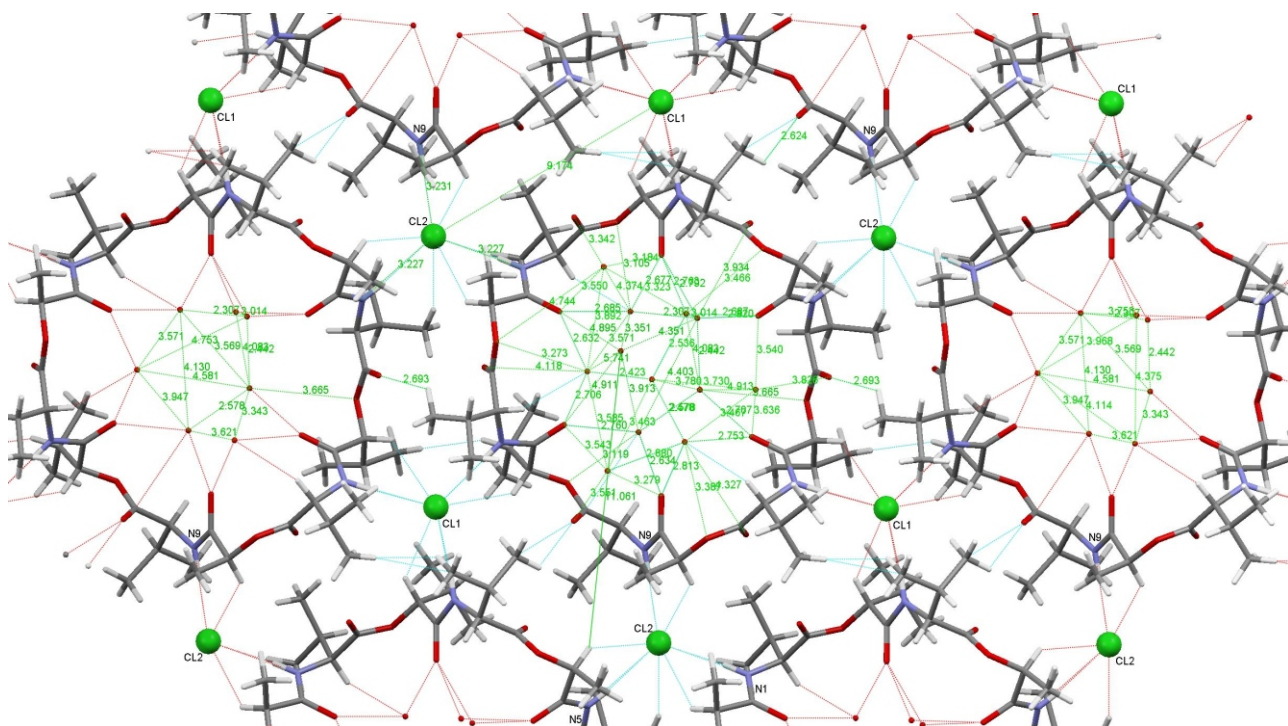


Figure 1. A single layer of valinomycin molecules in the valinomycin-HCl-water complex with stoichiometry 1:1:12. In the central valinomycin ring, all water molecules in the tunnel are shown. In the side rings, only the water molecules directly bound to the valinomycin molecule are present. Stability of the structure is strengthened by chloride ions (small balls) fixed in all cases to three amine groups of three neighbor valinomycin molecules.

deposited in the CCDC except a single one have very low accuracy of structure determination (R-factors are in the interval 9 % – 19 %). The only exception is a complex of valinomycin with a single water molecule and 1,5-dioxan determined by Lang in 1992 ($R = 3.8\%$). Surprisingly, none of the structures solved by now was with higher water content. Therefore, we determined two structures with different numbers of water molecules per single molecule of valinomycin.

Newly determined structures

In the new structures, a single valinomycin molecule is complexed with two waters ($R = 4.2\%$) or with 12 water molecules ($R = 8.5\%$). The results show that the macrocycle of a single valinomycin folds into a shape similar to the seam on a tennis ball. In this way, it forms a large barrel with hydrophobic external surface (formed by side chains of all monomers) and a large hydrophilic cavity inside the barrel with 12 carbonyls and 6 ether oxygens. In case that hydrophilic cavity has small volume, the cavity is more spherical. In the case of higher content of water, the cavity swells and takes an elongated ellipsoidal shape.

The solved structures show clearly that water molecules concentrate inside the valinomycin cavity. In excess of water, two valinomycins form a dimer of the elongated barrel shape filled by at least 24 water molecules. The external surface of the barrel formed by all side chains of both valinomycin molecules is highly hydrophobic and therefore the complexes stack side by side to form layers similar to a membrane. In other words, the whole system tends to form bilayers of valinomycin dimers. It is in agreement with the fact that the measured single crystal with higher

water content is formed by parallel stacking of these bilayers. Figure 1 shows a perpendicular view on a single layer of the above mentioned bilayer.

Valinomycin in the lipid membrane

The pattern formed in the high-water-content structure is an excellent model for valinomycin action in the cell membrane. Some of single valinomycin molecules sit on the surface of cell membrane forming thus small cavities and decreasing locally the thickness of membrane. Other valinomycin molecules form dimers inserted inside the membrane similarly to those described in the crystal structure. The valinomycin dimers (barrels with hydrophobic external surface and filled by solution) form water-filled tunnels across the membrane allowing the passive transport of ions or small molecules with good affinity for the cavity interior offering 24 carbonyls and 12 ether oxygens for hydrogen bonding on its surface.

These observations explain the mechanism of the valinomycin activity in the selective transport of ions and small hydrophilic molecules across the cell membrane. The study brings better understanding of the processes taking place in living organisms.

Acknowledgement

The work was supported by projects GA ČR 305/07/1073 and GA AV ČR IAA500500701.

1. F.H. Allen, *Acta Crystallogr.*, **B58**, (2002), 380-388.